

Bayesian Inference of Networks Across Multiple Sample Groups and Data Types Supplementary Materials

ELIN SHADDOX*, CHRISTINE B PETERSON, FRANCESCO C STINGO, NICOLA A. HANANIA,
CHARMION CRUICKSHANK-QUINN, KATERINA KECHRIS, RUSSELL BOWLER, MARINA
VANNUCCI*

¹*Department of Statistics, Rice University, Houston, TX, USA*

²*Department of Biostatistics, UT MD Anderson Cancer Center, Houston, TX, USA*

³*Department of Statistics, Computer Science, Applications “G. Parenti”, University of Florence,
Florence, Italy*

⁴*Department of Medicine-Pulmonary, Baylor College of Medicine, Houston, TX, USA*

⁵*Department of Pharmaceutical Sciences, School of Pharmacy, University of Colorado, Denver, CO,
USA*

⁶*Department of Biostatistics and Informatics, Colorado SPH, University of Colorado, Denver, CO, USA*

⁷*Department of Medicine, National Jewish Health, Denver, CO, USA*

elin@rice.edu, marina@rice.edu

APPENDIX A: DETAILS ON MCMC ALGORITHM FOR POSTERIOR INFERENCE

Updating Ω_{sk} : To sample Ω_{sk} , we rely on the block Gibbs sampler proposed in Wang (2015). For simplicity, assume each group’s data is column centered. The likelihood for each group is then

$$\mathbf{X}_{sk} \sim N(0, \Omega_{sk}^{-1}) \text{ where } s = 1, \dots, S \text{ and } k = 1, \dots, K$$

For the posterior full conditional of Ω_{sk} ,

$$P(\Omega_{sk} | \mathbf{X}_{sk}, \mathbf{G}_{sk}) \propto |\Omega_{sk}|^{n_{sk}/2} \exp\{-tr(\mathbf{X}_{sk}^T \mathbf{X}_{sk} \Omega_{sk})\} \times \prod_{i < j} \left\{ \exp\left(\frac{\omega_{skij}^2}{2\nu_{g_{skij}}^2}\right) \right\} \prod_{i=1}^P \left\{ \exp\left(-\frac{\lambda}{2} \omega_{skii}\right) \right\}$$

*To whom correspondence should be addressed.

Partitioning Ω_{sk} into $V = (v_{ij}^2)$ a $p \times p$ symmetric matrix with zeroed diagonal entries and $(v_{ij}^2)_{i < j}$ in the upper diagonal entries where $S = \mathbf{X}_{sk}^T \mathbf{X}_{sk}$ we can focus on the last column and row to acquire

$$\Omega = \begin{pmatrix} \Omega_{1,1} & \omega_{1,2} \\ \omega'_{1,2} & \omega_{2,2} \end{pmatrix}, \quad S = \begin{pmatrix} S_{1,1} & s_{1,2} \\ s'_{1,2} & s_{2,2} \end{pmatrix}, \quad V = \begin{pmatrix} V_{1,1} & v_{1,2} \\ v'_{1,2} & 0 \end{pmatrix}.$$

Then the conditional distribution of the last column in Ω_{sk} is

$$P(\omega_{12}, \omega_{22} | \mathbf{X}_{sk}, \mathbf{G}_{sk}, \Omega_{11}) \propto (\omega_{22} - \omega'_{12} \Omega_{11}^{-1} \omega_{12})^{n_{sk}/2} \exp \left[-\frac{1}{2} \left\{ \omega'_{12} D^{-1} \omega_{12} + 2s'_{12} \omega_{12} + (s_{22} + \lambda) \omega_{22} \right\} \right]$$

where $D = \text{diag}(v_{12})$. Then, changing variables from $(\omega_{1,2}, \omega_{2,2})$ to $(u = \omega_{1,2}, v = \omega_{2,2} - \omega'_{1,2} \Omega^{-1} \omega_{1,2})$ we have full conditionals

$$u | \cdot \sim N(-C s_{1,2}, C) \text{ and } v | \cdot \sim \text{Gamma} \left(\frac{n}{2} + 1, \frac{s_{2,2} + \lambda}{2} \right),$$

where $C = \{(s_{2,2} + \lambda) \Omega_{1,1}^{-1} + \text{diag}(v_{1,2}^{-1})\}^{-1}$. Using this method, we can permute any column to attain the full conditional used to generate $\Omega_{sk} | \mathbf{G}_{sk}, \mathbf{X}_{sk}$.

Updating \mathbf{G}_{sk} : Our full conditional on \mathbf{G}_{sk} is then an independent Bernoulli of the form

$$P(g_{skij} = 1 | \Omega_{sk}, \mathbf{X}_{sk}) = \frac{N(\omega_{skij} | 0, \nu_1^2) \pi}{N(\omega_{skij} | 0, \nu_1^2) \pi + N(\omega_{skij} | 0, \nu_0^2) (1 - \pi)}$$

where $\frac{\pi}{1-\pi}$ is determined by the MRF prior on the graph structure such that

$$\frac{\pi}{1-\pi} = \frac{P(\mathbf{G}'_{sk} | \nu_{sij}, \Theta_s, \{\mathbf{G}_{sm}\}_{m \neq k})}{P(\mathbf{G}_{sk} | \nu_{sij}, \Theta_s, \{\mathbf{G}_{sm}\}_{m \neq k})} = \exp \left\{ -(\nu_{sij} + 2 \sum_{m \neq k} \theta_{skm} g_{smij}) \right\}$$

for proposed new graph \mathbf{G}'_{sk} which differs from the current graph \mathbf{G}_{sk} in that only edge (i, j) is excluded from \mathbf{G}'_{sk} and included in \mathbf{G}_{sk} .

Updating ν_{sij} : Given the terms in the joint prior on graphs $\mathbf{G}_{s1}, \dots, \mathbf{G}_{sK}$ including ν_{sij} we have

$$\begin{aligned} P(\mathbf{G}_{s1}, \dots, \mathbf{G}_{sK} | \nu_{sij}, \Theta_s) &= \prod_{i < j} C(\nu_{sij}, \Theta_s)^{-1} \exp(\nu_{sij} \mathbf{1}^T \mathbf{g}_{sij} + \mathbf{g}_{sij}^T \Theta_s \mathbf{g}_{sij}) \\ &\propto C(\nu_{sij}, \Theta_s)^{-1} \exp(\nu_{sij} \mathbf{1}^T \mathbf{g}_{sij}) \end{aligned}$$

Then we can find the posterior full conditional

$$P(\nu_{sij} | \cdot) \propto P(\nu_{sij}) P(\Psi | X) \propto \frac{\exp(\nu_{sij} (a + \mathbf{1}^T \mathbf{g}_{sij}))}{C(\nu_{sij}, \Theta_s) (1 + e^{\nu_{sij}})^{a+b}}$$

For each (i, j) pair in $1 \leq i < j \leq p$, we then propose a value q^* from the density $\text{Beta}(a^*, b^*)$ and set $\nu^* = \text{logit}(q^*)$. Then the proposal density can be written in terms of ν^* as

$$q(\nu^*) = \frac{1}{B(a^*, b^*)} \frac{e^{a^* \nu^*}}{(1 + e^{\nu^*})^{a^* + b^*}}$$

Our Metropolis-Hastings ratio in the MCMC is then

$$r = \frac{P(\nu^* | \cdot) q(\nu_{sij})}{P(\nu_{sij} | \cdot) q(\nu^*)} = \frac{\exp[(\nu^* - \nu_{sij})(a - a^* + \mathbf{1}^T \mathbf{g}_{sij})] C(\nu_{sij}, \Theta_s) (1 + e^{\nu_{sij}})^{a+b-a^*-b^*}}{C(\nu^*, \Theta_s) (1 + e^{\nu^*})^{a+b-a^*-b^*}}$$

Updating θ_{skm} and γ_{skm} : We sample θ_{skm} and γ_{skm} from their joint posterior full conditional distribution. The terms in the joint prior on graphs $\mathbf{G}_{s1}, \dots, \mathbf{G}_{sK}$ including θ_{km} are

$$\begin{aligned} P(\mathbf{G}_{s1}, \dots, \mathbf{G}_{sK} | \nu_{sij}, \Theta_s) &= \prod_{i < j} C(\nu_{sij}, \Theta_s)^{-1} \exp(\nu_{sij} \mathbf{1}^T \mathbf{g}_{sij} + \mathbf{g}_{sij}^T \Theta_s \mathbf{g}_{sij}) \\ &\propto \prod_{i < j} C(\nu_{sij}, \Theta_s)^{-1} \exp(2\theta_{skm} g_{skij} g_{smij}) \end{aligned}$$

Given the prior on θ_{skm} and γ_{skm} , the posterior full conditional of θ_{skm} and γ_{skm} can be written

$$\begin{aligned} P(\theta_{skm}, \gamma_{skm} | \cdot) &\propto P(\mathbf{G}_{s1}, \dots, \mathbf{G}_{sK} | \nu_{sij}, \Theta_s) P(\theta_{skm} | \gamma_{skm}) P(\gamma_{skm} | \{\gamma_{tkm}\}_{s \neq t}, w_{km}, \Phi) \\ &\propto \left[\prod_{i < j} C(\nu_{sij}, \Theta_s)^{-1} \exp(2\theta_{skm} g_{skij} g_{smij}) \right] \times \left[(1 - \gamma_{km}) \delta_0 + \gamma_{km} \frac{\beta^\alpha}{\Gamma(\alpha)} \theta_{skm}^{\alpha-1} e^{-\beta \theta_{skm}} \right] \\ &\quad \times \frac{\exp(\gamma_{skm} (w_{km} + 2 \sum_{s \neq t} \phi_{st} \gamma_{tkm}))}{1 + \exp(w_{km} + 2 \sum_{s \neq t} \phi_{st} \gamma_{tkm})} \end{aligned}$$

Since the normalizing constant for the above mixture is analytically intractable, we use Metropolis-Hastings steps which sample θ_{skm} and γ_{km} for each pair (k, m) where $1 \leq k < m \leq K$ from their joint posterior full conditional distribution. The construction for this step follows in the manner of the MCMC approach described in [Gottardo and Raftery \(2008\)](#) for sampling from mixtures of mutually singular distributions. Two steps are performed at each iteration: a between-model move and a within-model move. This type of sampler has been shown in the literature to be effectively equivalent to a reversible jump Markov chain Monte Carlo (RJMCMC):

• For the between-model move, if the sampler has current state $\gamma_{skm} = 1$, we propose $\gamma_{skm}^* = 0$ and $\theta_{skm}^* = 0$. Otherwise, if in the current state $\gamma_{skm} = 0$, we propose $\gamma_{skm}^* = 1$ and sample θ_{skm}^* from the proposal density $q(\theta_{skm}^*) = \text{Gamma}(\theta_{skm}^* | \alpha^*, \beta^*)$. The Metropolis-Hastings ratio is

$$\begin{aligned} r &= \frac{P(\theta_{skm}^*, \gamma_{skm}^* | \cdot) q(\theta_{skm})}{P(\theta_{skm}, \gamma_{skm} | \cdot)} \\ &= \left[\prod_{i < j} \frac{C(\nu_{sij}, \Theta_s) \exp(-2\theta_{skm} g_{skij} g_{smij})}{C(\nu_{sij}, \Theta_s^*)} \right] \frac{\beta^{\alpha^*} \Gamma(\alpha)}{\beta^\alpha \Gamma(\alpha^*)} \theta_{skm}^{\alpha^* - \alpha} \frac{\exp((\beta - \beta^*)\theta_{skm})}{\exp(w_{km} + 2 \sum_{s \neq t} \phi_{st} \gamma_{kmt})} \end{aligned}$$

where Θ_s^* represents matrix Θ_s with entry $\theta_{skm} = \theta_{skm}^*$.

If in the current state $\gamma_{skm} = 0$, we propose $\theta_{skm}^* = 1$ and sample θ_{skm}^* from the proposal density specified before. When moving from $\gamma_{skm} = 0$ to $\gamma_{skm}^* = 1$, the Metropolis-Hastings ratio is

$$\begin{aligned} r &= \frac{P(\theta_{skm}^*, \gamma_{skm}^* | \cdot)}{P(\theta_{skm}, \gamma_{skm} | \cdot) q(\theta_{skm}^*)} \\ &= \left[\prod_{i < j} \frac{C(\nu_{sij}, \Theta_s) \exp(2\theta_{skm}^* g_{skij} g_{smij})}{C(\nu_{sij}, \Theta_s^*)} \right] \frac{\beta^\alpha \Gamma(\alpha^*)}{\beta^{\alpha^*} \Gamma(\alpha)} \theta_{skm}^{*\alpha - \alpha^*} \exp((\beta^* - \beta)\theta_{skm}^*) \exp(w_{km} + 2 \sum_{s \neq t} \phi_{st} \gamma_{kmt}) \end{aligned}$$

• We then perform a within-model move when the value of θ_{skm} sampled from the between-model move is 1. For this step, we propose a new value of θ_{skm} using the same proposal density as before. The Metropolis-Hastings ratio for this step is

$$\begin{aligned} r &= \frac{P(\theta_{skm}^*, \gamma_{skm}^* | \cdot) q(\theta_{skm})}{P(\theta_{skm}, \gamma_{skm} | \cdot) q(\theta_{skm}^*)} \\ &= \left[\prod_{i < j} \frac{C(\nu_{sij}, \Theta_s) \exp(2(\theta_{skm}^* - \theta_{skm}) g_{skij} g_{smij})}{C(\nu_{sij}, \Theta_s^*)} \right] \left(\frac{\theta_{skm}^*}{\theta_{skm}} \right)^{\alpha - \alpha^*} \exp[(\beta^* - \beta)(\theta_{skm}^* - \theta_{skm})] \end{aligned}$$

Updating w_{km} : Considering the terms of the joint prior on the vector $\gamma_{km} = [\gamma_{1km}, \dots, \gamma_{Skm}]^T$ including w_{km} we attain

$$P(\gamma_{km} | w_{km}, \Phi) \propto C(w_{km}, \Phi)^{-1} \exp(w_{km} \mathbf{1}^T \gamma_{km})$$

Then we can find the posterior full conditional for w_{km}

$$P(w_{km} | \cdot) \propto P(w_{km}) P(\Psi | \mathbf{X}) \propto \frac{\exp(dw_{km})}{(1 + e^{w_{km}})^{d+f}} C(w_{km}, \Phi)^{-1} \exp(w_{km} \mathbf{1}^T \gamma_{km}) \frac{\exp(w_{km}(d + \mathbf{1}^T \gamma_{km}))}{C(w_{km}, \Phi)(1 + e^{w_{km}})^{d+f}}$$

For each (k, m) pair in $1 \leq k < m \leq K$, we then propose a value q^{**} from the density $\text{Beta}(d^*, f^*)$ and set $w^* = \text{logit}(q^{**})$. Then the proposal density can be written in terms of w^* as

$$q(w^*) = \frac{1}{B(d^*, f^*)} \frac{e^{d^* w^*}}{(1 + e^{w^*})^{d^* + f^*}}$$

Our Metropolis-Hastings ratio in the MCMC is then

$$r = \frac{P(w^* | \cdot) q(w_{km})}{P(w_{km} | \cdot) q(w^*)} = \frac{\exp(w^* - w(d - d^* + \mathbf{1}^T \gamma_{km})) C(w_{km}, \Phi) (1 + e^{w_{km}})^{d+f-d^*-f^*}}{C(w^*, \Phi) (1 + e^{w^*})^{d+f-d^*-f^*}}$$

Updating ϕ_{st} and ζ_{st} : Our sampler for ϕ_{st} and ζ_{st} is constructed in a parallel manner to that for θ_{skm} and γ_{skm} . The terms in the joint prior on γ_{km} including ϕ_{st} are

$$P(\Gamma_{km} | w_{km}, \Phi) \propto \prod_{k < m} C(w_{km}, \Phi)^{-1} \exp(2\phi_{st} \gamma_{skm} \gamma_{tkm})$$

Given the priors on ϕ_{st} and ζ_{st} , the posterior full conditional can then be written

$$\begin{aligned} P(\phi_{st}, \zeta_{st} | \cdot) &\propto P(\gamma_{km} | w_{km}, \Phi) P(\phi_{st} | \zeta_{st}) P(\zeta_{st}) \\ &\propto \left[\prod_{k < m} C(w_{km}, \Phi)^{-1} \exp(2\phi_{st} \gamma_{skm} \gamma_{tkm}) \right] \times \left[(1 - \zeta_{st}) \delta_1 + \zeta_{st} \frac{\kappa^\eta}{\Gamma(\eta)} \phi_{st}^{\eta-1} e^{-\kappa \phi_{st}} \right] \\ &\quad \times u^{\zeta_{st}} (1 - u)^{(1-\zeta_{st})} \end{aligned}$$

For the between-model move, if in the current state $\zeta_{st} = 1$, we propose $\zeta_{st}^* = 0$ and $\phi_{st}^* = 0$. If in the current state $\zeta_{st} = 0$, we propose $\zeta_{st}^* = 1$ and sample ϕ_{st}^* from the proposal density $q(\phi_{st}^*) = \text{Gamma}(\phi_{st}^* | \eta^*, \kappa^*)$. When moving from $\zeta_{st} = 1$ to $\zeta_{st}^* = 0$, the Metropolis Hastings ratio is

$$\begin{aligned} r &= \frac{P(\phi_{st}^*, \zeta_{st}^* | \cdot) q(\phi_{st})}{P(\phi_{st}, \zeta_{st} | \cdot)} \\ &= \frac{\Gamma(\eta)}{\Gamma(\eta^*)} \frac{\kappa^{\eta^*}}{\kappa^\eta} \phi_{st}^{\eta^* - \eta} e^{(\kappa - \kappa^*) \phi_{st}} \left[\prod_{k < m} \frac{C(w_{km}, \Phi) \exp(-2\phi_{st} \gamma_{skm} \gamma_{tkm})}{C(w_{km}, \Phi^*)} \right] \frac{(1 - u)}{u} \end{aligned}$$

where ϕ^* represents the matrix ϕ with entry $\phi_{st} = \phi_{st}^*$. When moving from $\zeta_{st} = 0$ to $\zeta_{st}^* = 1$, the Metropolis-Hastings ratio is

$$\begin{aligned} r &= \frac{P(\phi_{st}^*, \zeta_{st}^* | \cdot)}{P(\phi_{st}, \zeta_{st} | \cdot) q(\phi_{st}^*)} \\ &= \frac{\Gamma(\eta^*)}{\Gamma(\eta)} \frac{\kappa^\eta}{\kappa^{\eta^*}} \phi_{st}^{(\eta - \eta^*)} e^{(\kappa^* - \kappa) \phi_{st}^*} \left[\prod_{k < m} \frac{C(w_{km}, \Phi) \exp(2\phi_{st}^* \gamma_{skm} \gamma_{tkm})}{C(w_{km}, \Phi^*)} \right] \frac{u}{(1 - u)} \end{aligned}$$

We then perform our within-model move when the value of ζ_{st} sampled from the between-model move is

1. For this step, we propose a new value of ϕ_{st} using the same proposal density as before. Our Metropolis-Hastings ratio step is then

$$r = \frac{P(\phi_{st}^*, \zeta_{st}^* | \cdot) q(\phi_{st})}{P(\phi_{st}, \zeta_{st} | \cdot) q(\phi_{st}^*)}$$

$$= \left[\prod_{k < m} \frac{C(w_{st}, \Phi) \exp(2(\phi_{st}^* - \phi_{st}) \gamma_{skm} \gamma_{tkm})}{C(w_{st}, \Phi^*)} \right] \left(\frac{\phi_{st}^*}{\phi_{st}} \right)^{\eta - \eta^*} \exp[(\kappa^* - \kappa)(\phi_{st}^* - \phi_{st})]$$

Appendix B: Case Study - Metabolite Selection

After matching our metabolite data to lipid and aqueous annotation files, we were able to extract KEGG IDs for each sample, yet were left with up to 67 metabolites matching to a single KEGG ID. Consequently, in order to reduce high correlation between covariates and improve interpretation of results, we selected a subset of less correlated covariates using a principal component analysis (PCA) procedure outlined below.

For example purposes, we provide sample code online generating correlated normal data for 20 subjects, using the Cholesky decomposition of the correlation matrix from a subset of 15 metabolites from the Regulation of Autophagy pathway which all matched to KEGG ID “C01194”. The steps for our selection procedure are as follows:

1. Read in data with variables as rows, observations as columns
2. Center and standardize data
3. Perform principal component analysis
4. Compute percent of variance contributed by each component
5. While first component explains less than 98%
 - a) Remove the least correlated variable into a `Removed` subset
 - b) Repeat Steps 2-4

6. Return the remaining Selected subset and the Removed subset, where Selected consists of more correlated variables, the first of which explains at least 98% of variance in PCA for the “Selected” subset
7. Repeat steps 1-6 with the Removed subset until no variables are remaining

After this procedure, the first variable for each iteration’s Selected subset is collapsed into a dataset for analysis. From the online example, the 15 correlated variables were collapsed into a subset of 7 less correlated variables for analysis after carrying out the procedure.

Appendix C: Case Study - Extended Hub Listings

Extended hub results for Regulation of Autophagy gene and metabolite platforms are given in tables 1 and 2, respectively, and those for Fc γ R-mediated phagocytosis in tables 3, 4, and 5.

APPENDIX D: CASE STUDY ON COPD DISEASE SEVERITY

Fc γ R

Estimated graphs for control, moderate, and severe subgroups for the Fc γ R-mediated phagocytosis (Fc γ R) pathway, obtained by selecting edges with MPPs greater than 0.5, are reported in Figures 1-2.

For the Fc γ R pathway, relative network similarities across subgroups, for the two platforms, were estimated as

$$MPP(\Theta)_{FcyR}^{Genes} = \begin{pmatrix} \cdot & 1.000 & 1.000 \\ & \cdot & 1.000 \\ & & \cdot \end{pmatrix} \quad MPP(\Theta)_{FcyR}^{Metabolites} = \begin{pmatrix} \cdot & .9547 & .9672 \\ & \cdot & .9499 \\ & & \cdot \end{pmatrix}$$

with relative similarity across platforms estimated as $MPP(\Phi)_{FcyR} = .9772$

Table 1. **Degree results for RegAuto Gene pathway:** Hub results for each compound in the pathway, as well as average, minimum, median, and maximum degree per node computed across all compound values for each disease subgroup. Hub nodes are those with degree ≥ 4 and genes involved in known protein protein interactions are denoted in **bold**.

Node Number	Compound	Degree G1	Degree G2	Degree G3
1	ULK3-225067_at	2	5	2
2	ATG3-221492.s.at	8	10	1
3	DRAM2-225228_at	4	9	3
4	ATG4D-226871_s.at	9	6	0
5	ATG14-204568.at	6	2	6
6	ATG16L2-229389_at	3	6	6
7	DRAM1-218627_at	5	10	1
8	ATG5-202512.s.at	4	8	7
9	ATG2A-213300_at	11	5	3
10	ULK2-204063.s.at	7	9	7
11	ATG13-203364_s.at	6	2	0
12	ATG4B-204903.x.at	4	3	4
13	ATG9A-202492_at	4	0	0
14	ATG4A-213115.at	1	8	2
15	EPG5-227638_at	3	7	4
16	ATG101-218214.at	5	5	2
17	ATG2B-226684_at	4	4	7
18	BECN1-208946.s.at	7	5	4
19	ATG10-223677.at	2	8	1
20	ATG12-213026.at	3	2	0
Average		4.9	5.7	3
Median		4	5.5	2.5
Min		1	0	0
Max		11	10	7

Distributions of Network and Platform Relatedness Parameters

To illustrate variability of network and platform relatedness parameters, posterior distribution histograms of non-zero values of Θ_S and Φ for the Regulation of Autophagy pathway are shown in Figures 3-5.

Biological Background for Pathways

Autophagy pathway When inspecting the hub listing, Autophagy related genes (ATG) typically showed decreased connectivity with severity (ATG2A, ATG3, ATG4D, ATG9A, ATG12, ATG13, ATG101) but

Table 2. **Degree results for Reg Auto Metabolite pathway:** Hub results for each compound in the pathway, as well as average, minimum, median, and maximum degree per node computed across all compound values for each disease subgroup. Hub nodes are those with degree ≥ 4

Node Number	Compound	Degree G1	Degree G2	Degree G3
1	PI(44:6)	4	2	3
2	1-Phosphatidyl-D-myo-inositol	2	1	4
3	PI(34:4)	5	3	3
4	PI(0-42:1)	1	0	2
5	PI(38:6)	4	3	5
6	PI(33:0)	1	2	1
7	PI(37:1)	4	5	4
8	PI(36:2)	3	7	5
9	PI(20:4)	0	3	3
10	PI(40:8)	3	4	2
11	PE(33:0)	1	1	3
12	PE(41:7)	4	5	3
13	PE(34:2)	4	4	2
14	PE(20:0)	4	2	2
15	PE(41:5)	4	5	4
16	PE(P-36:4)	2	4	4
17	PE(P-40:5)	1	1	3
18	PE(P-38:5)	1	1	2
19	PE(42:8)	4	4	3
20	PE(P-38:6)	3	2	3
21	PE(P-36:1)	1	1	1
Average		2.67	2.86	2.95
Median		3	3	3
Min		0	0	1
Max		5	7	5

a few showed increased connectivity (ATG2B, ATG5, ATG16L2). In addition, BECN1 also showed decreased connectivity with severity. There were also known protein-protein interactions ([Radoshevich and others, 2010](#); [Qiu and others, 2013](#); [Huttlin and others, 2017](#)) that were decreased with severity among these gene hubs (ATG3-ATG12, ATG3-BECN1). In general, there is elevated autophagy in response to cigarette smoke exposure and in lung specimens from COPD subjects ([Ryter and others, 2010](#); [Chen and others, 2008](#)), and this pathway may be a potential therapeutic target for lung disease ([Nakahira and Choi, 2013](#)).

Four metabolites stood out in the hub listing. Phosphatidylethanolamine (PE) (33:0) and PE(P-40:5)

Table 3. **Degree results for Fc γ R Gene pathway:** Hub results for each compound in the pathway, as well as average, minimum, median, and maximum degree per node computed across all compound values for each disease subgroup. Hub nodes are those with degree ≥ 4 and genes involved in known protein protein interactions are denoted in **bold**. The remaining portion of the hub listing for this pathway is continued in Table 4

Node Number	Compound	Degree G1	Degree G2	Degree G3
1	PLA2G6-210647_x.at	18	10	13
2	LAT-209881_s.at	20	21	18
3	BIN1-202931_x.at	20	21	17
4	PAK1-230100_x.at	11	27	10
5	ARPC5L-226915_s.at	16	11	13
6	HCK-208018_s.at	12	23	17
7	AKT2-225471_s.at	17	15	11
8	MAPK1-212271.at	11	18	2
9	PIK3R1-212240_s.at	13	11	10
10	CRK-202225.at	19	23	10
11	SYK-226068.at	11	18	20
12	ASAP1-224791.at	13	14	14
13	PLCG2-204613.at	9	16	4
14	RAC1-208640.at	11	3	4
15	ARPC3-208736.at	13	8	5
16	MARCKS-225897.at	20	21	17
17	PRKCA-213093.at	9	8	6
18	FCGR2A-203561.at	16	19	15
19	PIK3CB-212688.at	18	14	21
20	ARPC5-211963_s.at	19	11	3
21	MAP2K1-202670.at	16	11	7
22	PIK3CG-239294.at	8	16	9
23	ARPC1B-201954.at	3	8	1
24	LYN-210754_s.at	21	20	11
25	MARCKSL1-200644.at	3	8	14
26	PIP5K1B-205632_s.at	12	15	13
27	VASP-202205.at	4	8	3
28	DOCK2-213160.at	3	12	7
29	ARPC1A-200950.at	19	14	12

were unaffected in controls and moderate COPD, but showed increased connectivity with other metabolites with severe COPD. Alternatively PE(20:0) and phosphatidylinositol (PI) (34:4) hub metabolites showed decreased connectivity from control to moderate COPD, but remained constant from moderate to severe COPD. The edges were then explored for connectivity and disruption. Six metabolite-metabolite connections stood out. PI(34:4)–PE(P-38:6), PE(20:0)–PE(42:8), and PI(40:8)–PE(20:0) were connected

Table 4. **Degree results for Fc γ R Gene pathway Continued:** Hub results for each compound in the pathway, as well as average, minimum, median, and maximum degree per node computed across all compound values for each disease subgroup. Hub nodes are those with degree ≥ 4 , genes involved in known protein protein interactions are denoted in red.

Node Number	Compound	Degree G1	Degree G2	Degree G3
30	PRKCD-202545_at	21	21	24
31	PTPRC-212588_at	5	13	1
32	ARF6-224788_at	13	16	10
33	PIP5K1A-207391_s_at	1	4	3
34	RPS6KB1-204171_at	16	14	8
35	GSN-200696_s_at	19	11	8
36	RAF1-201244_s_at	1	2	0
37	PRKCB-209685_s_at	6	3	0
38	WAS-38964_r_at	4	1	1
39	CFL1-1555730_a_at	12	17	13
40	RAC2-213603_s_at	1	13	4
41	CDC42-208728_s_at	1	4	0
42	INPP5D-203332_s_at	28	22	18
43	LIMK1-204357_s_at	8	8	2
44	VAV1-206219_s_at	13	14	12
45	FCGR2B-210889_s_at	12	3	6
46	ARPC4-217818_s_at	11	15	11
47	WASF2-221725_at	7	17	11
48	ARPC2-208679_s_at	0	5	0
49	VAV3-218807_at	4	16	9
50	AKT3-212607_at	14	16	19
51	PIK3CA-204369_at	15	5	10
52	LIMK2-202193_at	9	12	6
53	PIK3CD-203879_at	9	15	8
54	PIK3R5-220566_at	13	14	13
55	PIP5K1C-212518_at	14	7	4
56	AKT1-207163_s_at	17	13	9
57	CRKL-212180_at	14	23	16
58	ARPC4-TTL3-211672_s_at	11	18	15
Average		11.79	13.21	9.45
Median		12	14	10
Min		0	1	0
Max		28	27	24

Table 5. **Degree results for Fc γ R Metabolite pathway:** Hub results for each compound in the pathway, as well as average, minimum, median, and maximum degree per node computed across all compound values for each disease subgroup. Hub nodes are those with degree ≥ 4

Node Number	Compound	Degree G1	Degree G2	Degree G3
1	DG(35:6)	6	3	3
2	DG(38:9)	1	2	1
3	DG(36:3)	4	3	4
4	DG(43:4)	2	3	2
5	DG(36:2)	4	4	7
6	DG(39:3)	1	2	1
7	DG(39:2)	4	5	3
8	DG(33:3)	0	2	0
9	DG(46:0)	6	3	5
10	DG(36:6)	4	3	1
11	DG(0-34:1)	4	2	7
12	DG(36:0)-d5 (internal standard)	4	5	3
13	Arachidonic acid	1	1	4
14	PA(24:0)	3	3	2
15	PA(0-28:0)	2	3	4
16	PA(0-34:1)	1	3	2
17	PA(P-30:0)	5	2	4
18	PA(P-20:0)	4	3	4
19	PA(0-38:4)	4	3	1
20	PA(42:2)	5	7	4
21	PA(28:0)	3	2	3
22	PA(15:0)	1	0	1
23	Sphingosine 1-phosphate	3	4	4
Average		3.13	2.96	3.04
Median		4	3	3
Min		0	0	0
Max		6	7	7

in the control group but these interactions were disrupted in the moderate and severe subgroups. The PI(40:8)–PE(42:8) connectivity was absent in controls and present in the moderate and severe subgroups. Finally, PI(38:6)–PE(P-38:6) and PE(42:8)–PE(P-36:1) were only connected in the severe subgroup. These compounds are all glycerophospholipids. Glycerophospholipids are part of lung surfactant and have been reported to be perturbed in COPD ([Telenga and others, 2014](#)). The increase in connectivity or the disruption of connections may suggest the transition to alternate routes due to pathway compensation as a consequence of disease.

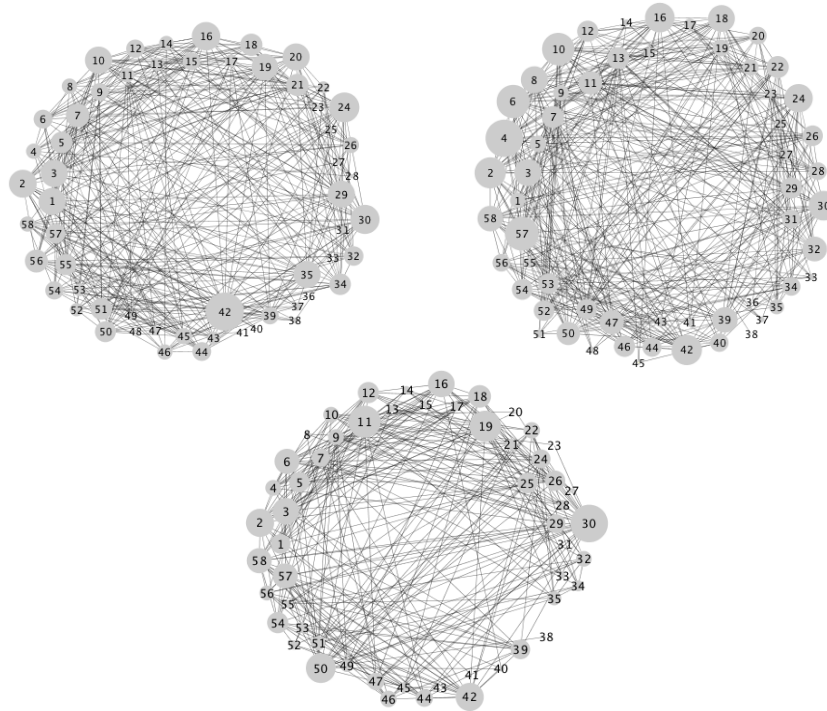


Fig. 1. $Fc\gamma R$ -mediated phagocytosis ($Fc\gamma R$) pathway, gene platform: Estimated graphs for control (top left), moderate (top right), and severe (bottom) subgroups, obtained by selecting edges with MPPs greater than 0.5. The size of the nodes is proportional to their degree.

Fc γ R-mediated phagocytosis pathway In the $Fc\gamma R$ -mediated phagocytosis pathway, two gene families stood out as important in the hub listing (AKT and PRKC). All three of the AKT family genes showed either decreased connectivity with COPD severity (AKT1, AKT2) or increased connectivity (AKT3). Phosphatase and tensin homolog (PTEN) is a regulator of the AKT signaling pathway, and genetic variation in PTEN is associated COPD (Hosgood and others, 2009). When selected edges with any of the AKT genes were explored for gene-gene interactions, many connections were broken in the moderate and severe subgroups of known protein-protein interactions to the AKT genes (AKT1-PIK3CA, AKT1-PIK3CB, AKT1-RPS6KB1, AKT2-PIK3CB, AKT1-AKT2). Many of these connections were with phosphoinositide-3-kinase (PI3K) genes. The PI3K pathway is activated by nicotine and plays a role in the pathology of COPD (Medina-Tato and others, 2007). Furthermore, there is evidence of miRNA targeting of PI3KCA transcripts that may contribute to initiation of COPD (Shi and others, 2015). The Protein Kinase C (PRKC)

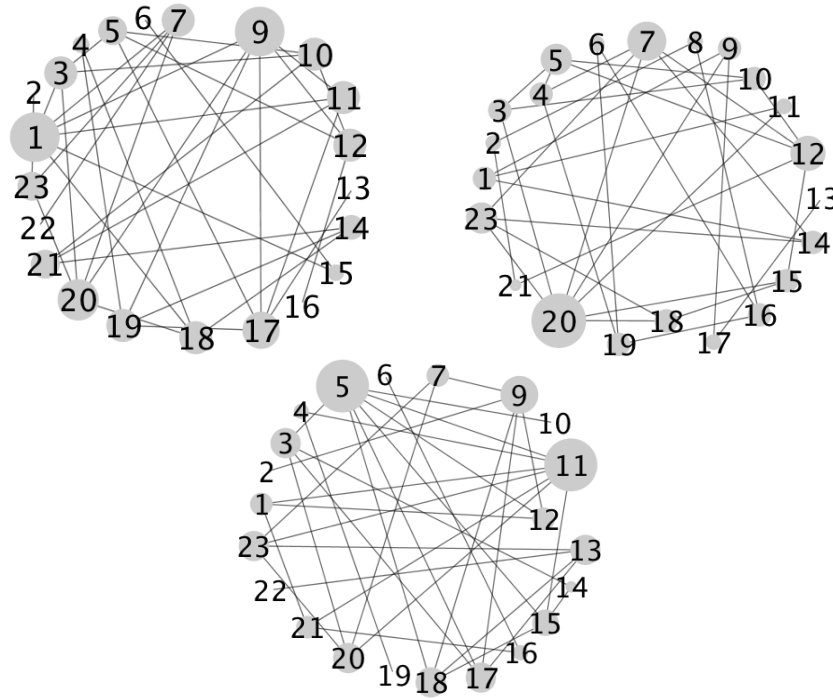


Fig. 2. $\text{Fc}\gamma\text{R}$ -mediated phagocytosis ($\text{Fc}\gamma\text{R}$) pathway, metabolite platform: Estimated graphs for control (top left), moderate (top right), and severe (bottom) subgroups, obtained by selecting edges with MPPs greater than 0.5. The size of the nodes is proportional to their degree.

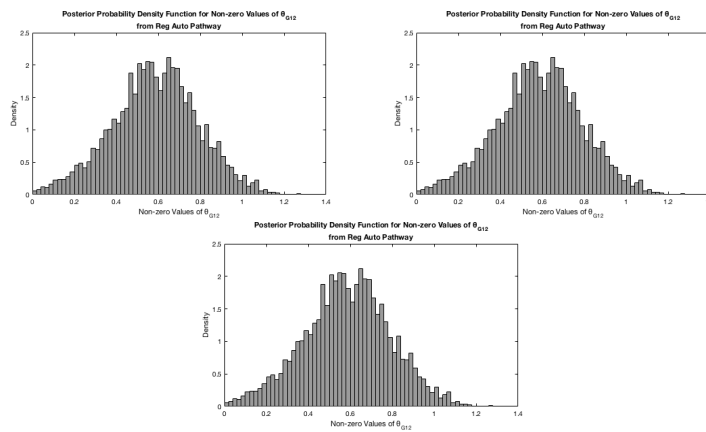


Fig. 3. Regulation of Autophagy (RegAuto) pathway, gene platform: posterior distributions of non-zero values for off-diagonal elements of Θ , providing relative similarity of subgroups for the gene platform.

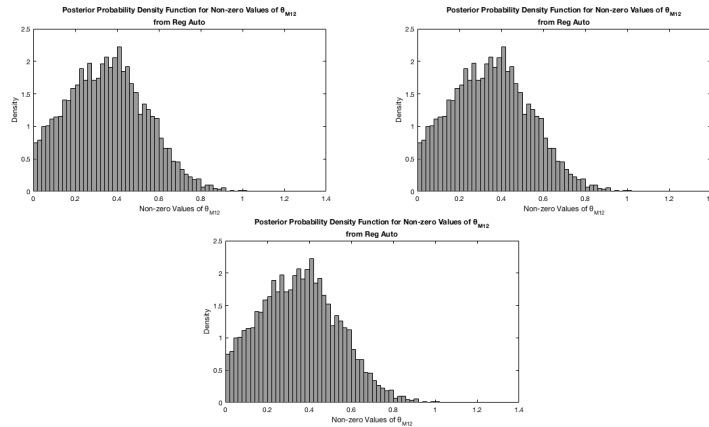


Fig. 4. Regulation of Autophagy (RegAuto) pathway, metabolite platform: posterior distributions of non-zero values for off-diagonal elements of Θ providing relative similarity of subgroups for the metabolite platform

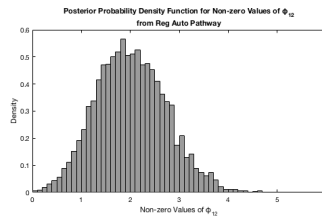


Fig. 5. Posterior distribution of non-zero values for Φ_{12} providing relative similarity of platforms

family is the other gene family that showed either decreased connectivity with severity (PRKCA, PRKCB) or increased connectivity (PRKCD). PRKC isoenzymes are expressed in human lung and tracheal smooth muscle (Webb and others, 1997). Furthermore, PRKCA has increased expression in pulmonary artery smooth muscle cells of smokers with COPD compared to non-smokers (Xaing and others, 2010). There was one gene-gene interaction (PRKCA-PLCG2) with one of the PRKC genes that was disrupted in the more severe COPD groups and was a known protein-protein interaction (Wang and others, 2006).

Three metabolites stood out as important in the hub listing for the FC γ R pathway. The hub metabolite diacylglycerol (DG) (35:6) showed decreased connectivity with disease severity, while the DG(36:2) and arachidonic acid hub metabolites showed increased connectivity with disease severity. When selected edges were explored for metabolite-metabolite interactions, many connections were broken in

the moderate and severe groups while connections, absent in the control and moderate subgroups, were present in the severe subgroup. Some notable examples include the following: the DG(46:0)–phosphatidic acid (PA) (42:2) interaction was disrupted with disease severity while the DG(36:3)–PA(42:2) was completely disrupted in the severe subgroup. The DG(38:9)–sphingosine-1-phosphate connection was only present in the control subgroup with no interactions in the moderate and severe group. Other notable interactions are DG(O-34:1)–sphingosone-1-phosphate, arachidonic acid–PA(P-20:0), arachidonic acid–PA(15:0), and arachidonic acid–sphingosine -1-phosphate; these connections were only present in the severe group. DGs are one of the constituents of pulmonary surfactant ([Lopez-Rodriguez and Perez-Gil, 2014](#)) and a disruption in surfactant is observed in COPD ([More and others, 2010](#)) and emphysema ([Cruickshank-Quinn and others, 2014, 2017](#)). Arachidonic acid is increased in COPD due to its production by inflammatory cells ([Barnes, 2016; Jamalkandi and others, 2015](#)) while sphingosine-1-phosphate accumulation in COPD is caused by cigarette smoke exposure ([Petrache and Petrusca, 2013](#)).

Appendix E: Simulation - Sensitivity Analysis

For sensitivity analysis, we generated data based on simulation setting one and $p = 80$ and studied the impact on cross-group and cross-platform relative similarity across differing hyperparameter values. We first looked at sensitivity by varying u , the Bernoulli indicator of relatedness across platforms, η and κ , the hyperparameters on the gamma slab of the mixture prior on Φ , while keeping the other parameters fixed as specified in the main paper. Resulting marginal posterior probability for Θ and Φ are given in Table 6. For platform one (the ‘gene’ platform), shared edge similarity for groups 1 and 2 was between 89% to 92% while for groups 1 and 3 it was around 23% and for groups 2 and 3 about 24%. For the second platform (the ‘metabolites’ platform), groups 1 and 2 and 1 and 3 shared approximately 91% and 90% of edges while groups 2 and 3 share approximately 81% of edges. Consequently, we determined that trial 1 from Table 6 resulted in relative similarity that was the most representative of our simulation set up, and therefore set $u = .1$, $\eta = 4$, and $\kappa = 5$ for future simulations and applications. Next, we looked at the

Table 6. Sensitivity Analysis: Inferred marginal posterior probability of Θ and Φ for varying u , η , and κ values.

Trial	u	η	κ	θ_{G12}	θ_{G13}	θ_{G23}	θ_{M12}	θ_{M13}	θ_{M23}	Φ
1	.1	4	5	1	.513	.5115	1	1	.999	.767
2	.5	4	5	1	.5585	.5775	1	1	1	.945
3	.9	4	5	1	.531	.639	1	1	.997	.996
4	.1	1	9	1	.1405	.1965	1	1	.9965	.151
5	.1	4	9	1	.2145	.2385	1	1	1	.4535
6	.5	4	9	1	.259	.326	1	1	1	.8115
7	.5	1	9	1	.151	.182	1	1	.9975	.576

Table 7. Sensitivity Analysis: Inferred marginal posterior probability of Θ and Φ are given for varying α , β , a , and b .

Trial	α	β	a	b	θ_{G12}	θ_{G13}	θ_{G23}	θ_{M12}	θ_{M13}	θ_{M23}	Φ
1	1	9	1	19	1	1	1	1	1	1	.9945
2	4	5	1	19	1	1	1	1	1	1	.994
3	1	9	1	4	.149	.002	.0045	.1915	.11	.033	.372
4	1	9	1	10	1	.9545	.9805	1	1	1	.9845
5	1	9	1	6	1	.139	.148	1	.9935	.9685	.5485
6	1	9	1	5	.994	.0425	.0285	.954	.87	.5495	.461
7	1	9	1	7	1	.51	.5105	1	1	.998	.764
8	1	9	1	8	1	.762	.7995	1	1	1	.903
9	1	9	2	7	.776	.014	.008	.7465	.4435	.1825	.41
10	4	5	2	7	.3675	.077	.0765	.424	.2625	.178	.3765

marginal posterior probability for Θ and Φ for different combinations of values for the hyperparameters α , β , a , and b , keeping u , η and κ as specified above. Results are given in Table 7. Based on those results, we determined to use Trial 7 values for our simulations and application, setting $\alpha = 1$ and $\beta = 9$ for the gamma slab portion of the mixture prior of cross group super graphs Θ_s , and setting $a = 1$, $b = 7$ for the prior on the sparsity parameter of the MRF prior linking networks within each platform.

Appendix F: Simulations - Power Analysis

To analyze the improvement of power attained through joint inference from our method, we compared the true positive rates across all methods for fixed false positive rates of .10 and .05. Results are given in table 8. For lasso methods, true positive rates were acquired by selecting the similarity parameters

which resulted in maximum AUC for each simulation as reported in the manuscript and then varying the sparsity parameter to attain the TPR which corresponded to the FPR threshold. As expressed in the table, our method is able to acquire a higher TPR for both settings in the $p = 80$ scenario, and in setting 2 of the $p = 40$ scenario our method performs better than both the fused and hub lasso methods; the higher TPR achieved by our method in some scenarios shows our method has provided improvement in terms of statistical power.

Appendix G: Case Study - Sensitivity Analysis

Graph Learning To study impact of hyper parameter settings on graph learning, we analyzed sensitivity of inferred networks for the Regulation of Autophagy pathway with 20 unique genes and 21 metabolites. These networks are compared in terms of sparsity levels as well as overlap with reported results from our paper.

As seen in tables 9, 10, and 11, hyper parameter settings have very little impact on graph learning performance and inferred network structure remains fairly stable across varying settings. In contrast, varying hyper parameters can cause quite an impact on inferred marginal posterior probabilities for Θ and Φ parameters, however ordering is generally preserved even as magnitude changes, and as these parameters are interpretable primarily on a relative scale we selected the hyper parameter settings that seemed to best reflect the true similarity for our simulation settings which are of the same approximate size as our data.

Relative Similarity Measures Hyperparameter settings and relative Similarity Measures Θ_S and Φ are listed in tables 12, 13, 14 for all trials. As these parameters are relative measures, final hyper parameter settings were determined as those which reflected the true similarity for our simulation settings which were of approximate size to the data.

Table 8. Simulation study: In setting one, one group on one of the two platforms is dissimilar from the others. In setting two, both platforms have dissimilar groups. True positive rates are reported as Mean over 25 replicates for $p = 80$ scenarios and 50 replicates for $p = 40$ scenarios.

Setting one, $p = 40$		
Method	FPR = .10	FPR = .05
Fused Lasso	0.843	0.779
Group Lasso	0.849	0.780
Hub Group Lasso	0.752	0.619
Multi-Platform Bayes	0.801	0.717

Setting two, $p = 40$		
Method	FPR = .10	FPR = .05
Fused Lasso	0.757	0.675
Group Lasso	0.831	0.753
Hub Group Lasso	0.761	0.641
Multi-Platform Bayes	0.817	0.735

Setting one, $p = 80$		
Method	FPR = .10	FPR = .05
Fused Lasso	0.926	0.680
Group Lasso	0.945	0.631
Hub Group Lasso	0.900	0.659
Multi-Platform Bayes	1.000	1.000

Setting two, $p = 80$		
Method	FPR = .10	FPR = .05
Fused Lasso	0.804	0.621
Group Lasso	0.883	0.629
Hub Group Lasso	0.903	0.662
Multi-Platform Bayes	1.000	1.000

REFERENCES

- BARNES, P.J. (2016). Inflammatory mechanisms in patients with chronic obstructive pulmonary disease. *J Allergy Clin Immunol* **138**(1), 16–27.
- CHEN, Z.H., KIM, H.P., SCIURBA, F.C., LEE, S.J., FEGHALI-BOSTWICK, C., STOLZ, D.B., DHIR, R., LANDRENEAU, R.J., SCHUCHERT, M.J., YOUSEM, S.A., NAKAHIRA, K., PILEWSKI, J.M.,

Table 9. Sensitivity Analysis to determine impact of graph learning from u , the Bernoulli prior on indicators of platform similarity, and η and κ , the hyper parameters influencing the Gamma slab portion of the mixture prior on Φ . Comparison is reported as edge counts for subgroups within each platform for each trial as well as the count of matching indicators when comparing adjacency matrices of learned networks vs the reported networks for each subgroup. As gene networks consist of 20 variables and metabolite networks have 21 variables, maximum matching indicator counts are 400 and 441 respectively for gene and metabolite subgroups.

Trial	Count Edges						Count Matching Indicators					
	G1	G2	G3	M1	M2	M3	G1	G2	G3	M1	M2	M3
1	128	136	88	77	85	89	388	386	386	441	437	439
2	122	134	84	79	83	91	392	384	386	439	439	441
3	120	128	98	77	85	85	390	386	384	441	437	435
4	112	126	82	75	83	93	386	384	380	439	439	439
5	114	132	84	77	83	89	388	386	382	441	439	435
6	122	132	86	77	85	89	388	386	384	441	441	435
7	124	126	90	75	85	89	386	388	384	439	437	439

Table 10. Sensitivity Analysis to determine impact of graph learning from α and β , hyper parameters for the slab portion of the mixture prior on off-diagonal entries of Θ_S linking sample groups within a platform, as well as a and b , the hyper parameters for the sparsity parameter of the MRF prior linking networks within each platform. Comparison is reported as edge counts for subgroups within each platform for each trial as well as the count of matching indicators when comparing adjacency matrices of learned networks vs the reported networks for each subgroup. As gene networks consist of 20 variables and metabolite networks have 21 variables, maximum matching indicator counts are 400 and 441 respectively for gene and metabolite subgroups. Trial 7 has hyper parameter settings equivalent to those reported in the document.

Trial	Count Edges						Count Matching Indicators					
	G1	G2	G3	M1	M2	M3	G1	G2	G3	M1	M2	M3
1	124	134	86	77	85	87	390	384	392	441	441	437
2	124	138	90	81	85	89	394	384	380	437	441	435
3	120	124	86	79	85	87	386	386	392	435	441	437
4	122	136	90	81	85	85	388	382	384	437	441	435
5	114	126	86	79	85	89	388	384	388	439	441	435
6	120	132	80	75	85	89	386	390	378	439	441	439
7	122	126	86	77	85	91	400	400	400	441	441	441
8	124	130	90	79	85	89	390	392	392	439	441	435
9	126	138	92	79	87	93	388	384	382	439	439	439
10	130	142	94	83	85	95	384	384	384	435	441	437

Table 11. Sensitivity Analysis to determine impact of graph learning from d and f , the hyper parameters for the sparsity parameter of the MRF prior linking platforms. Comparison is reported as edge counts for subgroups within each platform for each trial as well as the count of matching indicators when comparing adjacency matrices of learned networks vs the reported networks for each subgroup. As gene networks consist of 20 variables and metabolite networks have 21 variables, maximum matching indicator counts are 400 and 441 respectively for gene and metabolite subgroups.

Trial	Count Edges						Count Matching Indicators					
	G1	G2	G3	M1	M2	M3	G1	G2	G3	M1	M2	M3
1	122	128	92	75	87	89	384	390	390	439	439	439
2	126	130	90	79	85	87	388	388	388	439	441	437
3	122	130	90	79	85	93	388	380	376	439	437	439

Table 12. Sensitivity Analysis: Inferred marginal posterior probability of Θ and Φ for varying u , η , and κ values while holding constant $\alpha = 1$, $\beta = 9$, $a = 1$, $b = 7$, $d = 1$, and $f = 19$.

Trial	u	η	κ	θ_{G12}	θ_{G13}	θ_{G23}	θ_{M12}	θ_{M13}	θ_{M23}	Φ
1	.1	4	5	.985	.958	.975	.921	.932	.928	.171
2	.5	4	5	.989	.963	.978	.930	.943	.937	.993
3	.9	4	5	.984	.968	.977	.926	.942	.936	.999
4	.1	1	9	.953	.852	.910	.724	.776	.766	.173
5	.1	4	9	.962	.865	.933	.792	.820	.806	.611
6	.5	4	9	.966	.899	.944	.836	.850	.834	.908
7	.5	1	9	.947	.850	.923	.756	.776	.760	.644

Table 13. Sensitivity Analysis: Inferred marginal posterior probability of Θ and Φ are given for varying α , β , a , and b while holding constant $u = .1$, $\eta = 4$, $\kappa = 5$, $d = 1$, and $f = 19$.

Trial	α	β	a	b	θ_{G12}	θ_{G13}	θ_{G23}	θ_{M12}	θ_{M13}	θ_{M23}	Φ
1	1	9	1	19	.999	.990	.998	.991	.992	.990	.991
2	4	5	1	19	.999	.990	.996	.989	.993	.991	.991
3	1	9	1	4	.817	.631	.742	.455	.434	.440	.551
4	1	9	1	10	.997	.982	.990	.971	.978	.970	.979
5	1	9	1	6	.967	.918	.950	.862	.881	.877	.900
6	1	9	1	5	.927	.844	.883	.735	.755	.731	.786
7	1	9	1	7	.982	.955	.978	.920	.932	.930	.949
8	1	9	1	8	.991	.972	.985	.954	.957	.948	.969
9	1	9	2	7	.918	.797	.871	.685	.683	.681	.740
10	4	5	2	7	.876	.721	.795	.570	.579	.550	.585

Table 14. Sensitivity Analysis: Inferred marginal posterior probability of Θ and Φ for varying d and f values while holding constant $u = .1$, $\eta = 4$, $\kappa = 5$, $\alpha = 1$, $\beta = 9$, $a = 1$, and $b = 7$.

Trial	d	f	θ_{G12}	θ_{G13}	θ_{G23}	θ_{M12}	θ_{M13}	θ_{M23}	Φ
1	1	4	.986	.956	.975	.926	.934	.933	.768
2	2	7	.987	.963	.975	.927	.933	.937	.813
3	1	7	.973	.957	.973	.917	.941	.928	.867

LEE, J.S., ZHANG, Y., RYTER, S.W. and others. (2008). Egr-1 regulates autophagy in cigarette smoke-induced chronic obstructive pulmonary disease. PLoS ONE **3**(10).

CRUICKSHANK-QUINN, C., MAHAFFEY, S., JUSTICE, M.J., HUGHES, G., ARMSTRONG, M., BOWLER, R.P., REISDORPH, R., PETRACHE, I. AND REISDORPH, N. (2014). Transient and persistent metabolomic changes in plasma following chronic cigarette smoke exposure in a mouse model. PLoS ONE **9**(7).

CRUICKSHANK-QUINN, C., POWELL, R., JACOBSON, S., KECHRIS, K., BOWLER, R.P., PETRACHE, I. AND REISDORPH, N. (2017). Metabolomic similarities between bronchoalveolar lavage fluid and plasma in humans and mice. Scientific Reports **7**(5108).

GOTTARDO, R. AND RAFTERY, A. (2008). Markov chain monte carlo with mixtures of mutually singular distributions. J. Comput. Graph. Stat. **17**(4), 949–975.

HOSGOOD, H. D., MENASHE, I., HE, X., CHANOCK, S. AND LAN, Q. (2009). Pten identified as important risk factor of chronic obstructive pulmonary disease. Respir Med **103**(2), 1866–1870.

HUTTLIN, E.L., BRUCKNER, R.J., PAULO, J.A., CANNON, J.R., TING, L., BALTIER, K., COLBY, G., GEBREAB, F., GYGI, M.P., PARZEN, H., TAM, J. SZPYT S., ZARRAGA, G., PONTANO-VAITES, L., SWARUP, S., WHITE, A.E., SCHWEPPE, D.K., RAD, R., ERICKSON, B.K., OBAR, R.A., GURUHARSHA, K.G., LI, K., ARTAVANIS-TSAKONAS, S., GYGI, S.P. and others. (2017). Architecture of the human interactome defines protein communities and disease networks. Nature **545**, 505–509.

- JAMALKANDI, S., MIRZAIE, M., JAFARI, M., MEHRANI, H., SHARIATI, P. AND KHODABANDEH, M. (2015). Signaling network of lipids as a comprehensive scaffold for omics data integration in the sputum of copd patients. Biochimica et biophysica acta **1851**(10), 1383–1393.
- LOPEZ-RODRIGUEZ, E. AND PEREZ-GIL, J. (2014). Structure-function relationships in pulmonary surfactant membranes: from biophysics to therapy. Biochimica et biophysica acta **1838**(6), 1568–1585.
- MEDINA-TATO, D.A., WARD, S.G. AND WATSON, M.L. (2007). Phosphoinositide 3-kinase signaling in lung disease: leucocytes and beyond. Immunology **121**(4), 448–461.
- MORE, J.M., VOELKER, D.R., SILVEIRA, L.J., EDWARDS, M.G., CHAN, E.D. AND BOWLER, R.P. (2010). Smoking reduces surfactant protein d and phospholipids in patients with and without chronic obstructive pulmonary disease. BMC Pulmonary Medicine **10:53**.
- NAKAHIRA, K. AND CHOI, A.M. (2013). Autophagy: a potential therapeutic target in lung diseases. Am J Physiol Lung Cell Mol Physiol **305**(2), L93–L107.
- PETRACHE, I. AND PETRUSCA, D.N. (2013). The involvement of sphingolipids in chronic obstructive pulmonary diseases. The Handbook of Experimental Pharmacology Handbook **216**, 247–264.
- QIU, Y., HOFMANN, K., COATS, J.E., SCHULMAN, B.A. AND KAISER, S.E. (2013). Binding to e1 and e3 is mutually exclusive for the human autophagy e2 atg3. Protein Sci. **22**, 1691–1697.
- RADOSHEVICH, L., MURROW, L., CHEN, N., FERNANDEZ, E., ROY, S., FUNG, C. AND DEBNATH, J. (2010). Atg12 conjugation to atg3 regulates mitochondrial homeostasis and cell death. Cell **142**, 590–600.
- RYTER, STEFAN W., LEE, SEON-JIN AND CHOI, AUGUSTINE M.K. (2010). Autophagy in cigarette smoke-induced chronic obstructive pulmonary disease. Expert Rev Respir Med **4**(5), 573–584.
- SHI, LIANG, XIN, Q., CHAI, R., LIU, L. AND MA, Z. (2015). Ectopic expressed mir-203 contributes

- to chronic obstructive pulmonary disease via targeting tak1 and pik3ca. Int J Clin Exp Pathol **8**(9), 10662–10670.
- TELENGA, E.D., HOFFMANN, R.F., T'KINDT RUBEN, HOONHORST, S.J., WILLEMSE, B.W., VAN OOSTERHOUT, A.J., HEIJINK, I.H., VAN DEN BERGE, M., JORGE, L., SANDRA, P., POSTMA, D.S., SANDRA, K. and others. (2014). Untargeted lipidomic analysis in chronic obstructive pulmonary disease. uncovering sphingolipids. Am J Respir Crit Care Med **190**(2), 155–164.
- WANG, H. (2015). Scaling it up: Stochastic search structure learning in graphical models. Bayesian Analysis **10**(2), 351–377.
- WANG, J., WANG, N., XIE, J., WALTON, S.C., MCKOWN, R.L., RAAB, R.W., MA, P., BECK, S.L., COFFMAN, G.L., HUSSAINI, I.M. and others. (2006). Restricted epithelial proliferation by lacritin via pkcalpha-dependent nfat and mtor pathways. J Cell Biol **174**, 689–700.
- WEBB, B.L., LINDSAY, M.A., SEYBOLD, J., BRAND, N.J., YACOUB, M.H., HADDAD, E.B., BARNES, P.J., ADCOCK, I.M. AND GIEMBYCZ, M.A. (1997). Identification of the protein kinase c isoenzymes in human lung and airways smooth muscle at the protein and mrna level. Biochem Pharmacol **54**(1), 199–205.
- XAIING, M., LIU, X., ZENG, D., WANG, R. AND XU, Y. (2010). Changes of protein kinase calpha and cyclin d1 expressions in pulmonary arteries from smokers with and without chronic obstructive pulmonary disease. J Huazhong Univ Sci Technolog Med Sci **30**(2), 159–164.

[Received August 1, 2010; revised October 1, 2010; accepted for publication November 1, 2010]